

Planar photonic crystal polarization splitter

Lijun Wu

Ultrafast Photonics Collaboration, School of Physics & Astronomy, University of St. Andrews, St. Andrews KY16 9SS, UK, and
Department of Physics, Hong Kong University of Science and Technology, Hong Kong

M. Mazilu, J.-F. Gallet, and T. F. Krauss

Ultrafast Photonics Collaboration, School of Physics & Astronomy, University of St. Andrews, St. Andrews KY16 9SS, UK

A. Jugessur and R. M. De La Rue

Department of Electronics and Electrical Engineering, University of Glasgow, Glasgow G12 8LT, UK

Received January 16, 2004

The differential dispersion relation for the E and H modes (TM-like and TE-like, respectively) in planar photonic crystals is used to control the polarization-dependent propagation of light. E - and H -polarized beams were separated by 10° after propagating through a $20\text{-}\mu\text{m}$ -long planar photonic crystal in the wavelength range from 1250 to 1300 nm. The plane-wave expansion calculation matches well with the experimental results. This result represents the first demonstration, to our knowledge, of a polarization splitter realized in a planar photonic crystal configuration in the near-infrared wavelength range operating solely in transmission mode.

© 2004 Optical Society of America

OCIS codes: 230.1360, 260.2030, 130.3120.

Many of the studies on photonic crystals (PhCs) have focused on new means of tailoring the emission and propagation of light by use of the photonic bandgap property, whereby the photon density of states is zero. A PhC with a full photonic bandgap resembles an insulator in which the Fermi energy lies in the energy gap. Besides being used as insulators, however, PhCs can also be employed as photonic conductors. Their interesting dispersive properties^{1,2} have already led to applications such as superprisms, supercollimators, spot-size converters,^{3–8} and other devices related to the birefringent properties of PhCs.^{9–11} Polarization-dependent propagation is another property of PhCs that can be usefully exploited, e.g., for polarization separation in polarization diversity systems, for polarization-based logic, or for polarization mode dispersion compensation. Several types of polarization beam splitter based on ridge waveguides have already been reported in the literature.^{12–15} These devices typically require several millimeters of interaction length, however, which makes them less attractive for integration.

Alternatively, one can exploit the differential bandgap of the two polarizations in PhCs that has been studied by several groups^{16–18} and that has also been suggested for beam splitter functionality.^{19–21} None of these, however, has discussed the anisotropy of the equifrequency dispersive surfaces (EFDSs) for the two orthogonal polarizations.

Here, we propose and demonstrate an ultracompact ($20\text{ }\mu\text{m} \times 7\text{ }\mu\text{m}$) planar PhC E - or H -mode splitter by applying these different EFDS properties. Our polarization splitter is realized in standard semiconductor technology and can be easily integrated with other planar photonic circuits. We observe good agreement with wave-vector diagrams based on the plane-wave expansion method.

The material used in our experiments is a GaAs/AlGaAs waveguide heterostructure perforated by a hexagonal array of holes as in previous experiments.^{4,5} The lattice constant of the hole array, a , is designed to be 320 nm. The device layout is as follows: A $5\text{-}\mu\text{m}$ -wide input waveguide is tilted at 15° from normal to the crystal edge (Fig. 1). To pick up the output light at the right angle and to minimize refractive effects at the output interface, the shape of the crystal area is designed to be a semicircle with a $20\text{-}\mu\text{m}$ radius. The $3\text{-}\mu\text{m}$ output waveguides extend

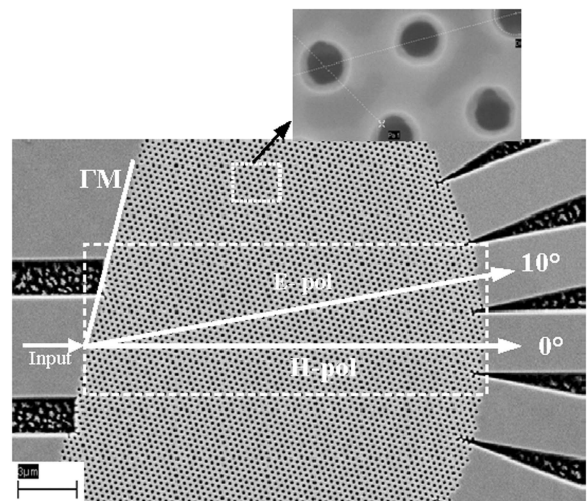


Fig. 1. Scanning electron micrograph (top view) of PhCs with input and output waveguides. The input waveguide is tilted 15° from normal to the crystal edge (the incident edge is $\Gamma - M$). The output waveguides are oriented at divisions of 10° . The inset highlights the small filling factor for this sample. Dashed square ($20\text{ }\mu\text{m} \times 7\text{ }\mu\text{m}$), required size for the device demonstrated.

somewhat into the crystal area and are oriented at divisions of 10° from -60° to 60° .

Vidicon micrographs of the output facet as a function of wavelength are shown in Fig. 2(a) (H polarization) and Fig. 2(b) (E polarization; H and E polarization will be shortened as H -pol and E -pol, respectively, in the following). Each spot represents one of the output waveguides that are spaced 10° apart, and the micrographs obtained for each wavelength are mounted together to show the evolution with wavelength. The corresponding transmission spectra are shown in Fig. 2(c) (H -pol) and Fig. 2(d) (E -pol), with the scattered points representing the raw data and solid curves being given as a visual aid. For H -pol [in Figs. 2(a) and 2(c)] the output light feeds into the 0° output waveguide in the wavelength range 1250–1365 nm, which means that the beam propagates straight through the PhC. For E -pol, in contrast, the beam feeds into the 10° output waveguide in the wavelength range 1250–1300 nm. Therefore the two polarizations are separated by 10° in the 1250–1300-nm wavelength range and the device acts as a polarization splitter. When the wavelength increases from 1300 to 1365 nm, the E -polarized beam swings from 10° back to 0° , which means that the two polarizations again travel along the same direction. The overall transmission that we measure is approximately 30% for an H -polarized beam and 10% for an E -polarized beam, normalized to an identical waveguide structure without the etched holes. This relatively high transmission, compared with values of 1–5% reported in our previous work,^{3–5} is mainly due to the smaller air-filling factor employed in the present devices. This lower filling factor is evident from the scanning electron micrograph provided as an inset in Fig. 1, and we believe that the lower filling factor reduces out-of-plane scattering, a point already stressed in Ref. 22. Note the superimposed oscillation of an approximately 30-nm period that leads to the pronounced intensity reduction of TE- 0° around 1325 nm in Fig. 1(c). We associate these dips with PhC Fabry–Perot-like interference from the two interfaces of the PhCs. Finite-size PhCs behave as Fabry–Perot etalons but show complex behavior because they can become resonant with any of the plane waves that constitute the PhC eigenmode. This behavior is further complicated because we operate in the second Brillouin zone, the input and output interfaces are not parallel, and beating occurs between different plane waves of the PhC eigenmodes. Therefore the observed 30-nm oscillation cannot be explained by a simple bulk Fabry–Perot effect alone, yet a full analysis would exceed the scope of this Letter.

To analyze the experimental results, the photonic band structures were calculated with the plane-wave expansion method, which is shown in Fig. 3. The light dashed lines show the operating position in this work. The wave-vector diagram or EFDSs were calculated from the band structure and used to map out the propagation directions of the Bloch waves in our PhCs. In the calculation a refractive index of 3.25 for the H mode and 3.05 for the E mode for the semiconductor host are

used. These refractive indices represent the effective index of the waveguide slab in the PhCs and were verified by identifying the photonic band edges in separate transmission measurements. The filling factor of the lattice was determined from scanning electron micrographs, so we used a value of 17% in the calculation. The propagation direction of light in the PhC

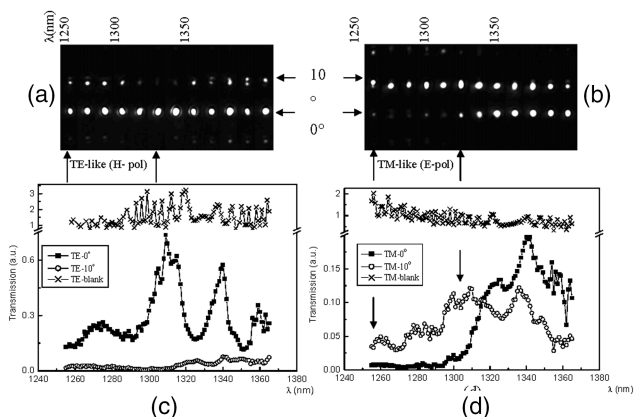


Fig. 2. (a), (b) Vidicon micrographs for the output light spots at different wavelengths for H - and E -polarized beams. (c), (d) Transmission spectra for the spots at 10° and 0° output waveguides and blank waveguides, respectively, with the scattered points representing the raw data. Solid curves are given as a visual aid. For an H -polarized beam [(a) and (c)] the output light is at 0° output waveguide from 1250 to 1365 nm, which means that the beam propagates through the PhCs straightforwardly. However, for an E -polarized beam the light transmits at 10° from 1250 to 1300 nm, which is 10° away from the propagation of an H -polarized beam. When the wavelength increases from 1300 to 1365 nm, the E -polarized beam swings from 10° to 0° , which means these two polarization-separated beams recombined after a wavelength bandwidth. The superimposed oscillation of an approximately 30-nm period that leads to the pronounced intensity reduction of TE- 0° around 1325 nm in (c) is possibly a Fabry–Perot effect caused by interface reflectivity. (More details are given in the text.)

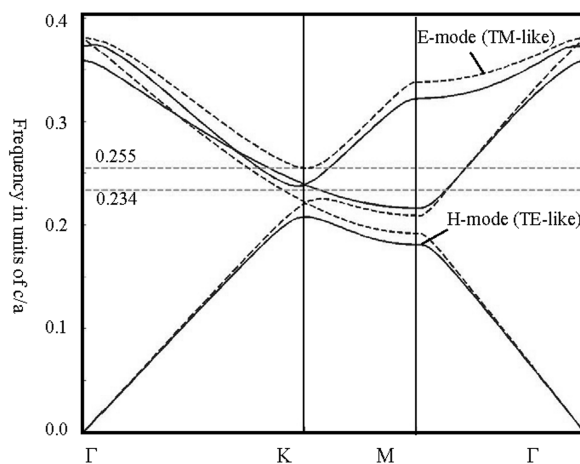


Fig. 3. Photonic band structures for an H and an E mode for the PhCs used in this demonstration. A plane-wave expansion method was used. The dashed horizontal lines correspond to the frequency range we used in the experiment.

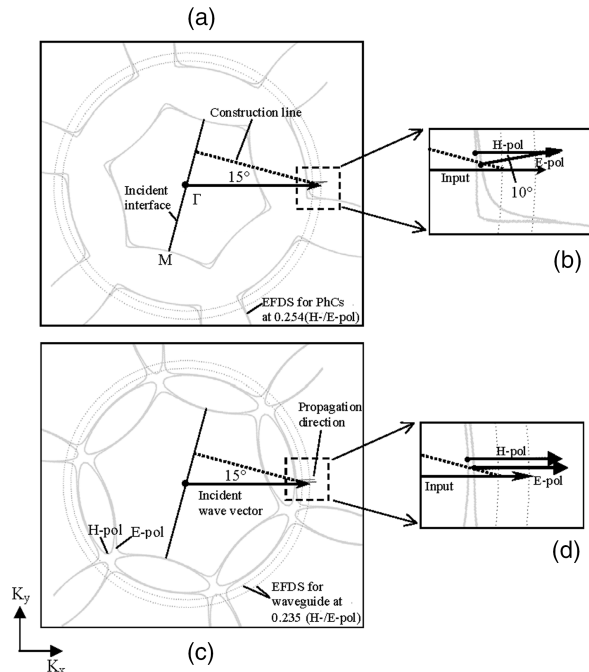


Fig. 4. (a)–(d) EDFs at frequencies of 0.254 and 0.235 c/a , which correspond to 1260- and 1360-nm wavelengths, for H mode and E mode, respectively. The diagrams on the left side represent the complete EDFs, and those on the right side represent the details of the incident and propagation directions. The graph clearly indicates that for the H mode the beam propagates straightforwardly through PhCs both at 1260 and 1360 nm, whereas for the E mode the beam propagates at 10° away from the H -polarized beam at 1260 nm and swings to the same direction as the H -polarized beam at 1360 nm.

is normal to the equifrequency contours, since the energy velocity is identical to the group velocity, which is given by $v_g = \nabla_{\kappa} \omega(\kappa)$.²³ With the momentum conservation rule (which is described in Ref. 6), the propagation direction can then be derived from the incident wave vector.

Figures 4(a) and 4(c) illustrate the calculation results at frequencies of 0.254 and 0.235 c/a , which correspond to 1260- and 1360-nm wavelengths, for the H mode and E mode, respectively. The diagrams on the left side represent the complete EDFs, and those on the right side represent the details of the incident and propagating beams. The graph clearly indicates that for H -pol the beam propagates straight through the PhC both at 1260 and 1360 nm, whereas for E -pol the beam propagates at 10° away from the incident angle at 1260 nm and swings back to straight propagation at 1360 nm. These numerical results closely agree with the experimental observations.

To summarize, we have used the differential dispersion of E and H modes in planar photonic crystals to control the polarization-dependent propagation of light. E - and H -polarized beams were separated by 10° after propagating through a 20- μm planar photonic crystal in the wavelength range of 1250–1300 nm. Plane-wave expansion calculation

matches well with the experimental results. We believe that this demonstration of a transmission-mode photonic crystal polarizing beam splitter is a useful addition to the tool kit of the nanophotonics circuit designer, following our previous demonstrations of superprisms and supercollimators in planar configuration in the near-infrared wavelength range.

We gratefully acknowledge the Glasgow University Nanoelectronics Research Centre for technical support and thank Tim Karle and Rab Wilson for useful discussions. L. Wu's e-mail address is phljwu@ust.hk.

References

1. M. Notomi, Phys. Rev. B **62**, 10696 (2000).
2. B. Gralak, S. Enoch, and G. Tayeb, J. Opt. Soc. Am. A **17**, 1012 (2000).
3. L. Wu, M. Mazilu, J. F. Gallet, and T. Krauss, Photonics Nanostruct. **1**, 31 (2003).
4. L. Wu, M. Mazilu, and T. Krauss, J. Lightwave Technol. **21**, 561 (2003).
5. L. Wu, M. Mazilu, T. Karle, and T. Krauss, IEEE J. Quantum Electron. **38**, 915 (2002).
6. H. Kosaka, T. Kawashima, A. Tomita, M. Notomi, T. Tamamura, T. Sato, and S. Kawakami, Phys. Rev. B **58**, R10096 (1998).
7. H. Kosaka, T. Kawashima, A. Tomita, M. Notomi, T. Tamamura, T. Sato, and S. Kawakami, Appl. Phys. Lett. **74**, 1212 (1999).
8. H. Kosaka, T. Kawashima, A. Tomita, T. Sato, and S. Kawakami, Appl. Phys. Lett. **76**, 268 (2000).
9. D. R. Solli, C. F. McCormick, R. Y. Chiao, and J. M. Hickmann, Opt. Express **11**, 125 (2003), <http://www.opticsexpress.org>.
10. F. Genereux, S. W. Leonard, H. M. van Diel, A. Birner, and U. Gosele, Phys. Rev. B **63**, 161101 (2001).
11. M. C. Netti, A. Harris, J. J. Baumberg, D. M. Whittaker, M. B. D. Charlton, M. E. Zoorob, and G. J. Parker, Phys. Rev. Lett. **86**, 1526 (2001).
12. S. M. Garner, V. Chuyanov, S. Lee, A. Chen, W. H. Steier, and L. R. Dalton, IEEE Photon. Technol. Lett. **11**, 842 (1999).
13. H. Maruyama, M. Hayuna, and H. Nishihara, J. Lightwave Technol. **13**, 1550 (1995).
14. P. Wei and W. Wang, IEEE Photon. Technol. Lett. **6**, 245 (1994).
15. R. M. de Ridder, A. F. M. Sander, A. Driessen, and J. H. J. Fluitman, J. Lightwave Technol. **11**, 1806 (1993).
16. E. Chow, S. L. Lin, S. G. Johnson, P. R. Villeneuve, J. D. Joannopoulos, J. R. Wendt, G. A. Vawter, W. Zubrzycki, H. Hou, and A. Alleman, Nature **407**, 983 (2000).
17. S. Foteinopoulou, A. Rosenberg, M. M. Sigalas, and C. M. Soukoulis, J. Appl. Phys. **89**, 824 (2001).
18. J. M. Hickmann, D. Solli, C. F. McCormick, R. Plambeck, and R. Y. Chiao, J. Appl. Phys. **92**, 6918 (2002).
19. Y. Ohtera, T. Sato, T. Kawashima, T. Tamamura, and S. Kawakami, Electron. Lett. **35**, 1271 (1999).
20. D. R. Solli, C. F. McCormick, R. Y. Chiao, and J. M. Hickmann, Appl. Phys. Lett. **82**, 1036 (2003).
21. S. Kim, G. P. Nordin, J. Cai, and J. Jiang, Opt. Lett. **28**, 2385 (2003).
22. T. F. Krauss, R. M. De La Rue, and S. Brand, Nature **383**, 699 (1996).
23. P. Yeh, J. Opt. Soc. Am. **69**, 742 (1979).